IEEE Open Journal of the Communications Society

Received 30 April 2023; accepted 15 May 2023. Date of publication 18 May 2023; date of current version 30 May 2023.

Digital Object Identifier 10.1109/OJCOMS.2023.3277782

Measuring EMF and Throughput Before and After 5G Service Activation in a Residential Area

LUCA CHIARAVIGLIO[1,2] (Senior Member, IEEE), STEFANIA BARTOLETTI[1,2], NICOLA BLEFARI-MELAZZI[1,2], CHIARA LODOVISI[1,2], ALESSIA MORETTI[3], FRANCESCO ZAMPOGNARO[1,2], AND MOHAMED-SLIM ALOUINI[4] (Fellow, IEEE)

[1]Department of Electronic Engineering, University of Rome Tor Vergata, 00133 Rome, Italy

[2]Consorzio Nazionale Interuniversitario per le Telecomunicazioni, Parma, Italy

[3]Freelance Cinematography and Film, Rome, Italy

[4]Computer, Electrical, and Mathematical Science and Engineering Division, King Abdullah University of Science and Technology, Thuwal 23955, Makkah Province, Saudi Arabia

CORRESPONDING AUTHOR: L. CHIARAVIGLIO (e-mail: luca.chiaraviglio@uniroma2.it)

This work was supported by the PLAN-EMF Project (KAUST) under Award OSR-2020-CRG9-4377.

ABSTRACT The deployment of 5G networks is approaching a mature phase in many countries across the world. However, little efforts have been done so far to scientifically compare ElectroMagnetic Field (EMF) exposure *and* traffic levels before and after the activation of 5G service over the territory. The goal of this work is to provide a sound comparative assessment of exposure and traffic, by performing repeated measurements before and after 5G provisioning service. Our solution is based on an EMF meter and a spectrum analyzer that is remotely controlled by a measurement algorithm. In this way, we dissect the contribution of each pre-5G and 5G band radiating over the territory. In addition, we employ a traffic chain to precisely characterize the achieved throughput levels. Results, derived from a set of measurements performed on a commercial deployment, reveal that the provisioning of 5G service over mid-band frequencies has a limited impact on the exposure. In parallel, the measured traffic is more than doubled when 5G is activated over mid-bands, reaching levels above 200 [Mbps]. On the other hand, the provisioning of 5G over sub-GHz bands does not introduce a substantial increase in the traffic levels. Eventually, we demonstrate that EMF exposure is impacted by the raw-land reconfiguration to host the 5G panels, which introduces changes in the sight conditions and in the power received from the main lobes.

INDEX TERMS 5G technology, EMF measurement, traffic measurement, comparative analysis.

I. INTRODUCTION

THE PROVISIONING of 5G service imposes to upgrade the currently deployed radio infrastructure, by installing new 5G antennas and by configuring the radio panels to provide the required levels of 5G coverage and capacity. The deployment of 5G has many benefits, such as improving data rates for smartphones and enabling innovative community services. However, part of the population is concerned about the potential impact of 5G antennas on the electromagnetic field (EMF) exposure that is radiated over the territory.

In this context, an interesting (and scientifically valid) question arises: Does the increase of throughput provided by the installation of 5G antennas escalate the exposure levels compared to pre-5G technologies? Or, in simpler words, What is the impact of a cellular tower upgrade from pre-5G to 5G on exposure and throughput levels over the surrounding areas? To the best of our knowledge, this question has not received sufficient attention by academic and regulator communities. In particular, previous works [1], [2], [3] mainly performed comparative exposure assessment between pre and post 5G installation without injecting any traffic.

Alternatively, another set of relevant works [4], [5], [6] evaluated EMF exposure by injecting traffic but without providing any analysis on the achieved throughput levels. In contrast to them, our work investigates the impact of 5G activation on EMF *and* performance in a commercial deployment.

We believe, in fact, that the comparative analysis of 5G exposure should be put in a wider picture that encompasses throughput analysis done in parallel to the EMF evaluation, for different reasons. First, 5G exposure is directly proportional to the achieved throughput levels, and hence evaluations without and with injected traffic are necessary to fully understand the (potential) EMF increase. Second, proving that 5G is exposure-friendly *and* at the same time able to increase throughput compared to pre-5G services may be a good driver towards a wider acceptance of such technology among the population.

The collection of EMF and throughput before and after 5G activation is hampered by several challenges, which include:

1) the adoption of dedicated spectrum portions by operators to provide pre-5G and 5G services - which have to be selectively monitored;
2) the need of carefully loading the wireless link between the base station and the terminal with large amount of traffic, in order to ensure that the exposure assessment is done under the maximum traffic condition;
3) the variation of EMF and performance that is experienced over the territory, which results from the propagation of mobile signals and the radio configuration of the base station antennas.

Our work explicitly tackles the previous challenges in the following ways:

1) we design a measurement framework composed of hardware (smartphones, dedicated server, wide-band meter, portable spectrum analyzer (SAN)) and software components to extensively measure EMF and throughput levels on the utilized spectrum portions before and after the activation of 5G service;
2) we select a set of meaningful locations in proximity to a multi-operator raw-land tower installation, based on the simulated exposure levels from the 5G installation;
3) we perform an extensive EMF and throughput measurement campaign over the locations in 2) before and after the tower upgrade to support 5G service.

Results reveal that the provisioning of 5G over mid-bands introduces a prompt increase of data rate compared to pre-5G services, with a limited impact on the exposure levels. Specifically, the normalized exposure per Megabit is substantially reduced in almost all locations when 5G is activated. This evidence reveals that more bits can be transported by 5G compared to 4G, with at the same time a limited impact on exposure. However, the (re)configuration of antenna panels upon 5G activation can introduce a local increase of exposure levels, e.g., due to the variation in the positioning, orientation, power and radiation diagram settings compared to pre-5G equipment. In addition, our work reveals that the largest source of exposure is still represented by pre-5G bands, even when 5G is active and downlink (DL) traffic is generated towards the measurement location. Eventually, the provisioning of 5G through sub-GHz bands does not introduce a consistent variation in the measured throughput levels, since the sub-GHz 5G spectrum portions are in reality mainly used to transport 4G signals.

As future work, we believe that our analysis should be extended in other countries and/or other portions of territory, in order to strengthen the outcomes and/or to characterize possible deviations on the observed patterns. As a side comment, we note that the installation of 5G antennas on the raw-land tower has a negative impact on the aesthetic of the surrounding environment. This aspect should be better tackled during the design of future mobile radio systems.

The rest of the paper is organized as follows. Related works are reviewed in Section II. The adopted methodology to evaluate exposure and throughput levels is described in Section III. The scenario under investigation is unveiled in Section IV. Section V analyzes in detail the results. Finally, Section VI summarizes our work and plans future research activities.

II. RELATED WORK

We divide the related work into the following taxonomies: *i*) in-situ measurements of 5G exposure, *ii*) long-term measurement of 5G/pre-5G exposure, *iii*) comparative studies of pre- and post- 5G exposure.

A. IN-SITU MEASUREMENT OF 5G EXPOSURE

The first category of works is tailored to studies that focused on the assessment of 5G exposure in close proximity to 5G installations [7], [8], [9], [10], [11], [12], [13], [14], [15], [16].

In more detail, Aerts et al. [7] proposed and evaluated a comprehensive measurement methodology for the assessment of EMF exposure in a 3.5 GHz 5G deployment. The authors included exposure assessments, based on the generation of active traffic towards the measurement location. Adda et al. [8] investigated 5G exposure at 3.6 GHz by evaluating a code-selective methodology. Aerts et al. [9] performed narrow-band measurement campaigns of 5G exposure from a commercial deployment. Chiaraviglio et al. [10] performed measurements with multiple tools (wide band meters, spectrum analyzers, smartphones) in proximity to a 3.6 GHz 5G installation located in a small town. Selmaoui et al. [11] measured exposure from 5G base stations in Korea by employing dosimeters. Wali et al. [12] and Chiaraviglio et al. [13] measured exposure levels from mm-Wave base stations for 5G mobile and 5G fixed wireless access (FWA) services, respectively. Colombi et al. [14] designed and evaluated a methodology for 5G exposure assessments over mm-Wave frequencies. Elbasheir et al. [15] evaluated exposure from a site up to 5G. Finally, Ursăchianu et al. [16] evaluated exposure from a commercial deployment including 5G base stations.

Overall, works [7], [8], [9], [10], [11], [12], [13], [14], [15], [16] provided solid indications about the limited impact of 5G exposure, even upon generation of traffic injected towards the measurement location. However, the presented results focused on exposure from an already operative 5G network, without shedding light on the EMF levels prior to 5G. In contrast to them, our work evaluates the exposure variations before and after 5G service activation. In addition, we explicitly include in our assessments the analysis of the measured throughput levels.

B. LONG-TERM MEASUREMENT OF 5G/PRE-5G EXPOSURE

The second category of studies [17], [18], [19] is tailored to the measurement of EMF exposure by adopting monitoring units. The goal of such studies was to perform long-term evaluations (over months/years) that could potentially capture exposure level variations due to the upgrade of the monitored base station(s). In more detail, Djuric et al. [17], [18] designed a continuous EMF monitoring system, which allowed measuring the exposure contributions from the different sources and their evolution over time. Chiaraviglio et al. [19] reported the outcomes of a long-term exposure monitoring lasting for several months, showing that the overall contribution of 5G with respect to legacy generations was limited.

Compared to [17], [18], [19], our work is different in terms of methodology. More concretely, we perform EMF assessments through spot measurements that are spread over the territory. In addition, previous works [17], [18], [19] are focused on passive EMF monitoring. In contrast to them, our work evaluates the impact of actively injecting traffic in the measurement location. Finally, we provide a comprehensive analysis about throughput variations.

C. COMPARATIVE STUDIES OF PRE- AND POST- 5G EXPOSURE

The third category of works is explicitly focused on a similar problem than ours, i.e., the comparative assessment of exposure before and after base station upgrade [1], [2], [3], [4], [5], [6].

In more detail, Markussen et al. [3] presented a very interesting dataset of measurements taken from different locations, which were repeated throughout the years. The authors demonstrated that exposure was overall limited across the locations, yet local variations (due, e.g., to network reconfiguration) were observed. Despite we recognize the importance of such work, we point out that the considered deployment did not include (yet) 5G base stations. In addition, throughput assessments were not performed.

Nedelcu et al. [2] and the Austrian forum of mobile communications [1] went one step further, by reporting comparative measurements before and after 5G deployment in Romania and in Austria, respectively. However, both works did not focus on active traffic generation. Moreover, the presented outcomes were mainly tailored to a wide-band EMF assessment, as the primary goal of [1], [2] was to compare the collected EMF levels against the limits. Differently from [1], [2], we evaluate exposure through a narrow-band approach, which allows dissecting the exposure contributions over the different bands. In addition, we explicitly focus on the joint assessment of EMF *and* traffic levels. However, similarly to [1], [2], we include a wide-band monitoring, in order to shed light on the total exposure values from all the sources that radiate over the measurement location.

Schilling et al. [6] provided an interesting comparative study of 5G exposure, including also active traffic generation. However, analysis about the achieved throughput across the measurement locations was not reported. A joint war-driving and in-situ comparative assessment was done by the Malta communication authority [5], but again not providing indications on the achieved throughput levels. Our work takes inspiration from [5], [6]. However, we go one step further by providing an in-depth analysis on the joint variations of EMF *and* throughput levels.

Finally, the closest work to ours is the analysis performed by the French national frequency agency, which conducted a nation-wide measurement campaign on the impact of 5G exposure, and published in 2021 a publicly available report [4]. Despite we share with such document different points (like the comparative nature of the study), our work is narrower in terms of scope (since we perform multiple measurements in one residential area) but wider and deeper in terms of assessments done in each measurement location. Our work includes, in fact, the evaluation of exposure without and with injected traffic. In addition, we compare performance before 5G and after 5G. Finally, we analyze 5G spectrum occupancy. The application of the methodology designed in our work to other areas - like the ones analyzed by [4] - is an interesting future work.

TABLE 1. Measurement objectives.

ID	Objective
O1	Temporal Repeatability
O2	Spatial Repeatability
O3	Frequency Selectivity
O4	Multiple-band Monitoring
O5	Traffic Saturation
O6	Site Selectivity
O7	5G Spectrum Occupancy
O8	Total Exposure Assessment

III. MEASUREMENT METHODOLOGY

We divide the presentation of the methodology into the following steps: *i*) definition of measurement goals, *ii*) overview of the equipment and tools, *iii*) description of SAN measurement algorithm, *iv*) description of the measurement procedures.

A. MEASUREMENT GOALS

We initially formalize a set of measurements goals, which are instrumental for the design of our framework. More concretely, Tab 1 reports the high level objectives, labeled

TABLE 2. Measurement SAN chain features.

Equipment	Feature	Value/Explanation
SAN	Model	Anritsu MS2090A
	Max. Frequency	32 GHz
	Used options	NRT spectrogram, RT spectrum analyzer
	Frequency samples	4001 (NRT), 501 (RT)
	Maximum RT BW	110 MHz
	RBW	Auto
	VBW	Auto
	Used interface	SCPI-based server
	Stored files	CSV Traces
Antenna	Model	Aaronia 6080
	Type	Directive
	Range	680 MHz - 8 GHz
	Gain	6 dBi (maximum)
RF Cable	Max Frequency	40 GHz
	Length	1 m
Laptop	Model	MacBook Air (M1-2020)
Connection Cable	Type	Ethernet Cat. 5E
	Length	1 m

with *O1*-*O8*. In more detail, *O1* defines temporal repeatability, since measurements have to be performed in each location before and after 5G service provisioning. Second, *O2* introduces the spatial repeatability, because the measurements have to be performed across different evaluation points spread over the territory. Third, *O3* ensures the frequency selectivity, because the contribution of 5G has to be dissected compared to the one of other technologies (like 4G). In addition, *O3* aims at distinguishing the contribution of a given operator compared to the other ones that radiate over the same area. Fourth, *O4* targets the monitoring across multiple spectrum portions, because carrier aggregation is employed for data transfers over 4G and 5G bands. Fifth, *O5* aims at achieving the traffic saturation over the wireless link between the base station and the terminal, in order to evaluate the exposure under the maximum traffic condition. Sixth, *O6* introduces the site selectivity, because we want to distinguish the exposure contributions from a given site with respect to the neighboring ones of the same operator that may provide coverage continuity. Seventh, *O7* introduces the monitoring of 5G spectrum occupancy - a detailed analysis that can provide fruitful indications about usage of the radio resources without and with injected traffic. Finally, *O8* defines the total exposure from the different operators and the different technologies that radiate over the same measurement location. Such analysis, which is orthogonal with respect to the previous goals, could provide fruitful indications that complement the narrow-band measurements.

B. EQUIPMENT AND TOOLS

We adopt three distinct equipment chains, namely: *i*) SAN chain, *ii*) wide band monitoring (WBM) chain, and *iii*) traffic chain. In more detail, SAN and WBM chains are used for the exposure measurement, while the traffic chain is used for both traffic generation and traffic measurement.

1) SAN CHAIN

The SAN chain, whose features are summarized in Table 2, is composed of a portable spectrum analyzer, which is equipped with multiple software options. In this work, we employ the non-real-time (NRT) spectrogram, which allows extracting directly the channel power vs. time from the considered frequency range. Moreover, we exploit the real-time (RT) spectrum feature, which allows recording the received power vs. frequency vs. time of the monitored spectrum. Both functionalities are instrumental for the extensive exposure assessment pursued in this work.[1] In addition, resolution bandwidth (RBW) and video bandwidth (VBW) are automatically tuned by the instrument. Eventually, the SAN is remotely controlled by an external laptop through the exchange of Standard Commands for Programmable Instruments (SCPI) commands, a set of instructions that allow running the measurement procedure directly in software.

The second chain component listed in Table 2 is the measurement antenna, which covers all mobile frequencies up to 8 [GHz]. The antenna manufacturer provides the gain vs. frequency diagram, which is used to extract the antenna factor and then to compute the power density / electric field out of the received power values. The antenna is connected to the SAN through a radio-frequency (RF) cable, whose short length allows limiting the impact of losses introduced by such component.

Overall, the SAN measurement chain allows achieving goal *O2*, since both SAN and control laptop are battery powered. In this way, the equipment guarantees the required spatial repeatability, because the instruments do not require electricity from the grid and they can be easily deployed across multiple measurement locations. In addition, the SAN adoption inherently allows performing frequency selective measurements (objective *O3*), as well as monitoring 5G spectrum occupancy (objective *O7*). Finally, the directive antenna allows achieving objective *O6*, as the main lobe is concentrated around the direction that is pointed by the equipment, i.e., the site under consideration.

TABLE 3. Measurement WBM chain features.

Equipment	Feature	Value/Explanation
Probe	Model	WaveControl WPF8
	Range	100 kHz - 8 GHz
	Technology	Isotropic - RMS Diode
	Sensitivity	0.2 V/m
	Resolution	0.02 - 0.1 V/m
Meter	Model	WaveControl SMP2
	Stored Files	Excel Traces

2) WBM CHAIN

The chain, whose features are summarized in Table 3, is made up of a tri-axial probe (mimicking an isotropic antenna) and a meter. The probe is able to cover the frequencies in use by 5G, with low sensitivity and resolution values. The meter is the central unit of the chain, which allows setting the measurement parameters. The WBM equipment is battery-powered, hence meeting objective *O2*. In addition, the total

1. In addition, the RT recording may be instrumental to detect jammers in hostile environments [20]. Moreover, it can be used to monitor the signal in joint communication and radar sensing architectures [21].

Algorithm 1 Narrow Band Measurement Algorithm (NBMEA)

Require: array of monitored frequencies $\mathbb{F}$, array of span widths $\mathbb{S}$, number of average channel power measurements N^{AVG}, initial time to compute the average channel power T^{INIT}, inter sample time T^{SAM}, number of samples per average channel power value N^{SAM}.

Ensure: matrix of power density values $\mathbb{P}$, matrix of EMF values $\mathbb{E}$, matrix of timestamp values $\mathbb{T}^{\text{STAMP}}$.

1: set_SAN_settings(N^{SAM}); *//Set RMS trace detector, rolling average type detector, number of samples to compute the channel power, reference level, scale div, pre-amplifier off, continuous sweeping*
2: N^{F}=size($\mathbb{F}$); *//retrieve total number of monitored frequencies*
3: **for** f = 1:N^{F} **do** *//Iterate over DL FDD and TDD frequency bands*
4: activate_chp_power($\mathbb{F}$(f), $\mathbb{S}$(f),T^{INIT});
5: **for** m = 1:N^{AVG} **do** *//Iterate over the sample measurements*
6: $\mathbb{P}$(f,m)= fetch_chp(); *//Retrieve current channel power measurement*
7: $\mathbb{T}^{\text{STAMP}}$(f,m)=fetch_timestamp(); *//Retrieve timestamp measurements*
8: pause(T^{SAM}); *//Trigger pause function*
9: **end for**
10: **end for**
11: $\mathbb{E}$=compute_emf($\mathbb{P}$); *//Compute EMF values from PD matrix*

TABLE 4. Traffic chain features.

Equipment	Feature	Value/Explanation
Server	Hardware	4 Intel Xeon ER-1230 (four cores) and 64 GB RAM
	OS	Ubuntu 18.04.1
	Traffic Generator	iPerf v3
Smartphone 1	Model	Samsung S20+ 5G
	Traffic Generator App	Magic iPerf
Smartphone 2	Model	Apple iPhone 12
	Traffic Generator App	iPerf 3 iOS

exposure in terms of electric strength is monitored, thus ensuring objective *O8*.

3) TRAFFIC CHAIN

The third and last chain realizes both traffic generation and traffic measurement, thus achieving objective *O5*. As detailed in Table 4, the chain is composed of a dedicated server and two smartphones. Both server and smartphones run the iPerf software, which allows generating synthetic traffic from a software agent installed on the server towards an App installed on the smartphone. The adoption of a dedicated server - running exclusively the iPerf server and installed at the University premises - allows guaranteeing (potentially) large throughput levels. In this way, we can saturate the radio link between the base station and the used smartphone.

C. SAN MEASUREMENT ALGORITHM

In order to assess the impact of pre-5G and 5G exposure, we need to perform monitoring over multiple bands. This is due to the fact that 5G typically employs dedicated spectrum portions compared to pre-5G technologies, like 4G. In addition, both 5G and pre-5G signals are spread across multiple bands, which are typically not contiguous. This is objective *O4*, which requires to perform the narrow-band monitoring over multiple bands. However, the implementation of such step with a manual setting of the SAN chain is an hard task - which would dramatically increase the measurement time. To solve such issue, in this work we rely on a completely softwarized measurement procedure, called NARROW BAND MEASUREMENT ALGORITHM (NBMEA). The algorithm is run on the laptop connected to the SAN. The low level commands of the algorithm are synthesized with SCPI format.

Algorithm 1 reports the pseudocode of NBMEA. The algorithm takes as input the set of frequencies $\mathbb{F}$ and the set of span values $\mathbb{S}$, which represent the center reference and the amplitude of the bands to be monitored, respectively. In addition, NBMEA requires a set of parameters to tune the measurement, including: *i*) the total number of values of average channel power N^{AVG}, *ii*) the initial waiting time to be ensured before capturing the first average channel power T^{INIT}, *iii*) the waiting time between two consecutive measurements of average channel power T^{SAM}, *iv*) the number of channel power samples to compute a single value of average channel power N^{SAM}.

The logic of NBMEA is rather simple. Initially, the set of SAN settings is implemented (line 1). Such parameters include: *i*) root mean square (RMS) trace detector, in accordance with relevant measurement standards [22], [23], *ii*) computation of the average channel power as a rolling temporal window - useful to detect spectrum variations across time, *iii*) number of samples to compute the channel power average - a tunable parameter passed as input to NBMEA, *iv*) initial reference level and scale division - instrumental to correctly display the signal on the SAN, *v*) deactivation of the pre-amplifier chain, as potentially the measured signal can be non-negligible, *vi*) activation of continuous sweeping.

In the following step, NBMEA iterates over the set of bands that have to be monitored (line 2-3). For each band, the channel power measurement is triggered (line 4), by passing to the function the current center frequency and the current

span. In addition, the T^{INIT} parameter is provided as input. In this way, the measured signal is stabilized before starting the saving of the sampled data. In the next part, an inner loop is performed over the samples that need to be captured (line 5). For each sample, a channel power measurement of power density is triggered (line 6), a timestamp recording is triggered (line 7), and a measurement pause, equal to T^{SAM} parameter, is imposed (line 8). When all the samples for all the bands have been recorded, the electric field for each sample and each band is computed as a post-processing step (line 11).

Overall, the time complexity of the algorithm grows linearly with the number of monitored bands and also linearly with the number of samples N^{AVG}. Focusing instead on space complexity, the channel power measurement allows dramatically reducing the size of the adopted structures. More specifically, a single value, corresponding to the average one, is used to represent the entire signal over the monitored band. However, we point out that the matrices used to record the measurements grow linearly with N^{AVG} parameter.

D. MEASUREMENT PROCEDURES

We describe hereafter the entire measurement procedures, which are divided into baseline vs. active traffic assessments. The former aims at measuring exposure level in the environment without injecting any traffic, while the latter includes the generation of active traffic towards the measurement location, in order to evaluate the exposure level under the most conservative conditions.

1) BASELINE ASSESSMENT

The Baseline Assessment (BA) procedure involves WBM and SAN chains. The following steps are performed: *Step 1*) SAN and WBM chains positioning, *Step 2*) Turn on SAN and WBM equipment, *Step 3*) Start EMF recording on WBM chain and start NBMEA, algorithm on SAN chain, *Step 4*) Wait for measurement time T (higher than execution time of NBMEA), *Step 5*) Stop recording on WBM *Step 6*) Turn off SAN and WBM chains.

At the end of BA, the WBM chain provides as output an exposure trace in Excel spreadsheet format, while the laptop controlling the SAN stores the output matrices including exposure data.

The BA procedure is then repeated for an interval of one minute with the SAN chain, in order to record the RT 5G spectrum vs. time. In this way, we collect information about 5G spectrum occupancy, thus ensuring objective *O7*.

2) ACTIVE TRAFFIC ASSESSMENT

The Active Traffic Assessment (ATA) procedure involves the generation of active traffic towards the measurement location. Consequently, the traffic chain is employed in parallel to the EMF SAN chain. As a side comment, the WBM chain is not employed in this case, because the WBM probe is not able to distinguish base station vs. smartphone exposure levels, especially when the smartphone generates traffic in close proximity to the probe. We remind in fact that our primary goal is to evaluate base station exposure, which is ensured by the SAN chain.

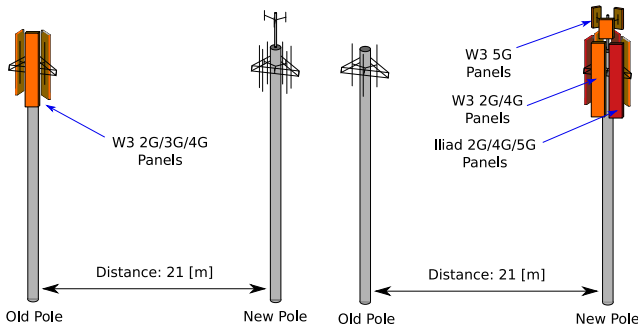

(a) Before 5G Activation. (b) After 5G Activation.

FIGURE 1. Breakdown of radiating panels and pole positioning before and after 5G activation.

The ATA procedure then consists of the following steps: *Step 1*) position SAN and traffic chains, *Step 2*) turn on SAN chain and smartphone, *Step 3*) start iPerf DL transfer towards the smartphone, *Step 4*) start NBMEA, *Step 5*) wait for NBMEA termination, *Step 6*) stop iPerf transfer, *Step 7*) turn off SAN equipment.

The smartphone used in the experiments is able to store the collected throughput vs. time trace on a comma-separated values (CSV) file. Similarly to the BA assessment, the laptop controlling the SAN stores the output matrices with the exposure measurements.

Finally, we repeat the ATA procedure by setting the RT recording of the 5G spectrum band(s) on the SAN chain. Clearly, the iPerf transfer in this case is stopped only when the RT recording is completed (i.e., after around one minute).

IV. BEFORE AND AFTER 5G SCENARIO

We initially unveil the characteristics of the raw-land under consideration, and then we shed light on the selected measurement locations.

A. RAW-LAND CHARACTERISTICS

We consider a raw-land tower installation located in Sacrofano, a small town in the neighborhood of Rome city (Italy). The tower hosts the W3 operator before 5G activation. After 5G activation, 5G coverage is provided by two distinct operators, namely W3 and Iliad. In parallel to 5G provisioning, Iliad also activates pre-5G services. More concretely, Fig. 1 sketches the panel positioning before and after 5G activation. Prior to 5G (Fig. 1(a)), a tri-sectorial set of W3 panels is installed on the pole, providing 2G/3G/4G coverage. After 5G (Fig. 1(b)) the pole is shifted of 21 [m], and a new set of panels is installed. In more detail, W3 installs three panels for legacy 2G/4G technologies, and a new set of small antennas is placed on top of the pole to provide signal coverage over 5G mid-band frequencies. On the other hand, Iliad provides 2G/4G/5G coverage with a

TABLE 5. Subset of FDD DL / TDD spectrum portions licensed to W3 before and after 5G provisioning (B = before 5G, A = after 5G, green = active band, coral = inactive band).

Scope	Technology	Frequency	Band
B, A	4G	796 [MHz]	10 [MHz]
B, A	2G/4G	955 [MHz]	10 [MHz]
B, A	4G	1850 [MHz]	20 [MHz]
B, A	4G	2120 [MHz]	20 [MHz]
B, A	4G	2680 [MHz]	20 [MHz]
B	4G	2585 [MHz]	20 [MHz]
A	4G	2585 [MHz]	20 [MHz]
B	5G	3447.5 [MHz]	20 [MHz]
B	5G	3547.5 [MHz]	20 [MHz]
B	5G	3610 [MHz]	20 [MHz]
A	5G	3590 [MHz]	60 [MHz]

TABLE 6. Subset of FDD DL / TDD spectrum portions licensed to Iliad before and after 5G provisioning (B = before 5G, A = after 5G, green = active band, coral = inactive band).

Scope	Technology	Frequency	Band
B	5G	763 [MHz]	10 [MHz]
A	5G	763 [MHz]	10 [MHz]
B,A	2G/4G	927.5	5 [MHz]
B,A	4G	1835	10 [MHz]
B,A	4G	2150	10 [MHz]
B,A	4G	2635	10 [MHz]
B,A	5G	3630	20 [MHz]

single set of panels, which are placed at the same height than the 2G/4G panels of W3.

In the following, we shed light on the considered set of frequencies adopted by operators before and after 5G installation. In this work, we are interested on Base Station (BS) exposure, and hence we target the monitoring of Frequency Division Duplexing (FDD) DL and Time-Division Duplexing (TDD) spectrum portions. Table 5 reports the frequency breakdown for W3 operator. The first column highlights the frequency scope (i.e., before or after) while the remaining ones detail the implemented technology, the center frequency and the bandwidth. Not surprisingly, most of spectrum portions are managed without changes by W3 before and after 5G activation. However, different exceptions emerge. In more detail, W3 has licensed (also in agreement with Fastweb operator) three distinct spectrum portions to provide 5G signal over mid-bands before 5G activation on the site. Obviously, such bands were not active on the site under investigation before 5G, as the set of panels installed on the pole (Fig. 1(a)) did not include any 5G equipment. Interestingly, a spectrum change has been implemented in parallel to the activation of 5G. This spectrum change was applied not only to the site under investigation, but also to the other installations in rural areas located in the same region. The resulting configuration provides 5G coverage over a contiguous portion of 60 [MHz] bandwidth, which can potentially realize huge capacity to users. Finally, the set of bands after 5G activation include a spectrum portion at 2585 [MHz], which is used to boost throughput levels for 4G connections.

Table 6 highlights the FDD DL or TDD spectrum portions licensed to Iliad operator. Compared to W3, Iliad has

FIGURE 2. View of the pre 5G and post 5G poles from private property (before 5G activation) - figure best viewed in colors.

a smaller set of bands in use for mobile technologies. In addition, the realized 5G bands on the site (upon activation of 5G) include a spectrum portion at 700 [MHz], which provides another difference compared to W3. As a side comment, Iliad has also licensed another 5G spectrum band at 3.6 [GHz], which is not provided by the site after 5G activation. This choice may be motivated by the fact that such band would require to install an additional set of panels, which would increase the installation costs for Iliad.

Fig. 2 shows pre 5G and post 5G poles from a ground level position, before 5G activation. The urbanization in the surroundings of the pole is relatively low, with different independent villas (like the one in the figure) that are located around the raw-land installation. Each property typically experiences Line-of-Sight (LoS) conditions with respect to both installations in most of outdoor zones, which can (potentially) receive non-negligible exposure levels from the cellular installation.

B. SELECTION OF THE MEASUREMENT LOCATIONS

In the following step, we select the candidate locations to perform the repeated measurements. In this work, we concentrate our attention on the outdoor locations of the private property shown in Fig. 2. This choice is motivated by the fact that the poles were visible from almost every point of the property, and therefore the owners were interested in a full exposure assessment. However, the new 5G pole was not (yet) operative at the time of measurement selection. Consequently, a complete simulation has been run, by considering the radio configuration of the post 5G installation. Our goal has been to find suitable measurement locations, characterized by non-negligible 5G exposure obtained from simulation.

Focusing on the simulation details, we have employed the ATDI HTZ Communications program [24]. The tool is a professional radio planning and optimization software currently in use by Italian operators and regulation authorities. The parameters that are passed as input to the

program include: *i*) complete radio configuration file, providing detailed information about electrical center height of each panel, panel orientation on the horizontal plane, panel mechanical/electrical tilting on the vertical plane, antenna maximum gain, antenna radiation diagram, antenna output power and antenna power scaling factor, *ii*) building layer, which is taken from OpenStreetMap, by selecting the region of interest with resolution of 2.5 [m], *iii*) clutter layer (including the information of the terrain types), taken again from OpenStreetMap, and *iv*) digital elevation model with step equal to 2.5 [m], taken from ATDI map server from `Italy:Rome` dataset.

We then launch the simulation by selecting the following options: *i*) deterministic model with diffraction geometry adopting the Deygout94 computation, *ii*) subpath attenuation set with area computation, and *iii*) evaluation distance equal to h_{UE}=0.93 [m] above ground level.[2] With these settings, the software computes the received electric field by applying a ray-tracing based model for each pixel of the considered map. The output of this step is a heatmap, like the one shown in Fig. 3(a). We then select a pair of measurement locations, detailed in Fig. 3(a) with pins numbered 1 and 2 (respectively). The selection is based on the accessible zones of the property that experience the highest simulated field level (red to white colors in the picture). The pin labeled with A in the figure marks instead the positioning of post-5G installation.

In addition, the simulation is repeated with $h_{\mathrm{UE}} = 4.93$ [m], corresponding to the height of the terraces at first floor of the building shown in Fig. 2. The outcome of this step is shown in Fig. 3(b). Both terraces are in LoS with respect to the pre-5G and 5G installation. This fact, coupled with the higher altitude than locations 1 and 2, may suggest that such points receive higher exposure levels than the outdoor locations at ground level. However, the building contour has an impact on the simulated field level. In particular, when the default building height is assumed, a simple cuboid is used to approximate the building profile in Fig. 2. Consequently, the exposure on the balcony locations (labeled as 3 and 4 pins in the figure) is not evaluated in the conditions actually experienced in reality, because both points are incorporated inside the building cuboid. Consequently, very low exposure levels are predicted from simulation on such locations. To solve such issue, we run again the program by imposing a building height equal to h_{BUILD}=4 [m]. Fig. 3(c) shows the outcome of the simulation. Interestingly, both locations lie outside the building cuboid, in LoS conditions. Consequently, higher exposure levels are predicted - thus justifying further analysis on locations 3 and 4 through real measurements on the field.

At the end of the procedure, a total of four measurement locations have been identified. The pictures of the locations are also shown in the subfigures of Fig. 4, which were taken

2. This setting is based on the actual height that is imposed during the measurements campaigns.

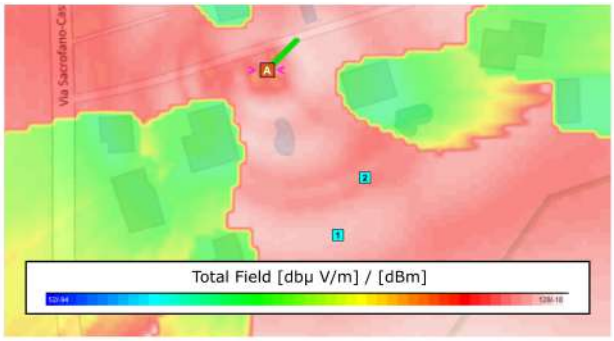

(a) h_{UE}=0.93 m.

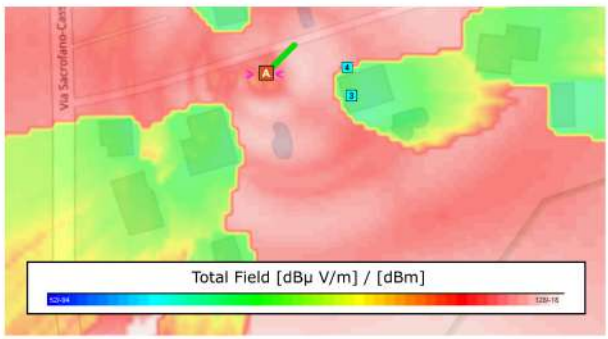

(b) h_{UE}=4.93 m and h_{BUILD}=10 m

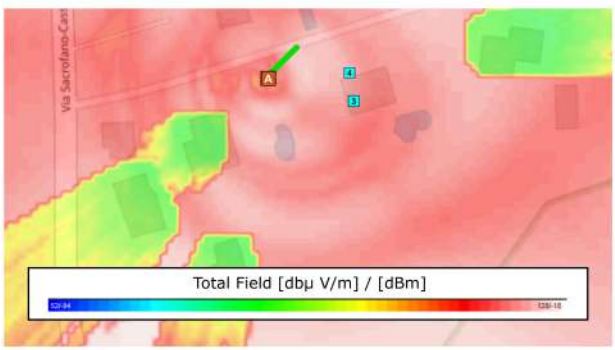

(c) h_{UE}=4.93 m and h_{BUILD}=4 m

FIGURE 3. Positioning of the measurement points w.r.t. the simulated exposure of the post 5G site - subfigures best viewed in colors.

before 5G installation. It is worth noting that all locations (except from location 4) are in LoS with respect to the pre-5G installation, and hence we expect that all of them also receive substantial exposure levels from the pre-5G pole. As a side comment, location 4 is in semi-LoS with respect to the pre-5G installation, since a tree partially obstructs the view. The impact of such condition is treated in detail when we perform measurements over such location.

To complete our overview of the scenario, Fig. 5 reports an aerial view with the measurement locations, the pre-5G and post-5G installation (labeled as B and A in the figure, respectively), and the sectorization of the panels (represented by colored arrows). In general, all measurement locations almost fall inside the main direction of at least one panel. In particular, locations 3 and 4 are mainly radiated by one

(a) Location 1. (b) Location 2.

(c) Location 3. (d) Location 4.

FIGURE 4. Pictures of the measurement locations 1-4 - subfigures best viewed in colors.

W3 sector. On the other hand, locations 1 and 2 are radiated by one sector of W3 and another one of Iliad after 5G activation. Overall, such findings confirm that the exposure over the selected locations should be always non-negligible after 5G activation.

V. RESULTS

We divide the presentation of our results in the following parts: *i*) timeline of measurements and tower upgrade steps, *ii*) settings of the measurement chains, *iii*) W3 analysis, *iv*) Iliad analysis, *v*) joint analysis of total exposure, and, finally, *vi*) 5G signal spectrum analysis.

A. MEASUREMENTS AND TOWER UPGRADE TIMELINE

Fig. 6 reports a scheme with the tower upgrade steps on the left and the performed measurements campaigns on the right. All measurements were performed during working days over 10:00-13:30 hours. In this way, exposure levels are evaluated during periods of time with non-negligible traffic levels generated by other users. Initially, we perform the BA assessment before the starting of the works on the new pole. This activity was carried out on 11th November 2022. The new Iliad antennas were installed shortly after - on 24th November. However, the new antennas were not yet operative at that time, due to the fact that complementary works like wiring and cabinet placing were not completed yet. Consequently, we perform the ATA assessment on 28th November, thus measuring the signal levels solely from the pre-5G pole. The W3 band change at 3.6 GHz was implemented shortly after - on 1st December 2022. The installation of the new W3 antennas was performed on 6th December

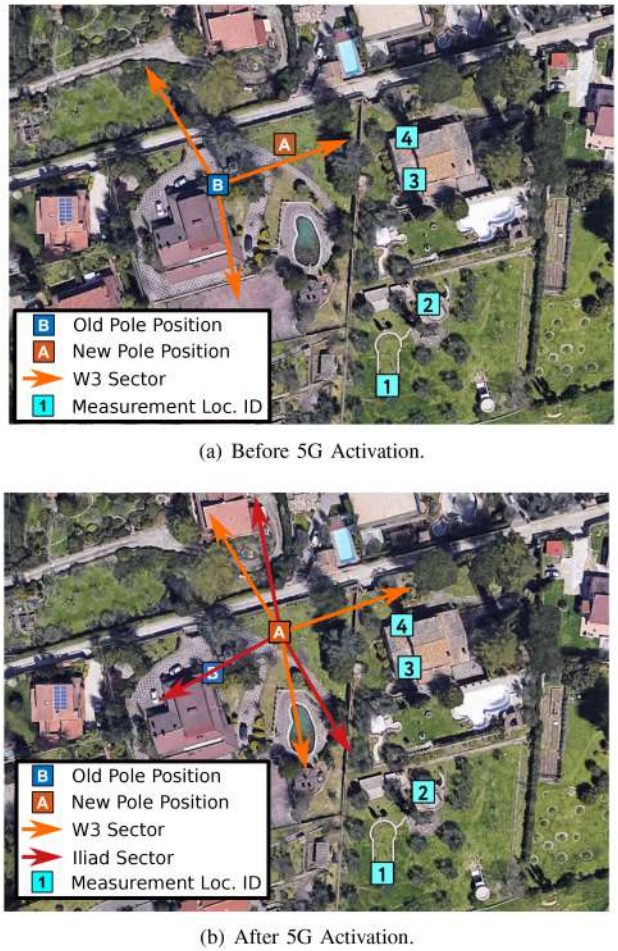

(a) Before 5G Activation.

(b) After 5G Activation.

FIGURE 5. Aerial view with sectorization and measurement points (source map: Google Earth) - subfigures best viewed in colors.

2022, which then became active on 13th December 2022, based on a CellMapper test that we conducted with the S20+ 5G smartphone. The new signal from Iliad was detected on 2nd January 2023, by running again the CellMaper application on the iPhone smartphone. Consequently, we perform the BA and ATA assessments of the post-5G installation on the same day. This step was instrumental to evaluate the impact of the new 5G signals generated by the antennas installed on the new pole.

B. MEASUREMENT CHAINS SETTINGS

We detail hereafter the settings of SAN chain, WBM chain and traffic chain. In addition, the input parameters setting for NMBEA algorithm is detailed.

1) SAN CHAIN AND NBMEA ALGORITHM SETTINGS

The SAN antenna is placed on a tripod, at a height of around 1 [m] from ground level, in order to minimize the effects of ground reflections. The antenna is then manually oriented to point towards the radiating set of antennas: before 5G activation towards the pre-5G pole and after 5G activation towards the post-5G pole. The SAN and the control laptop are then

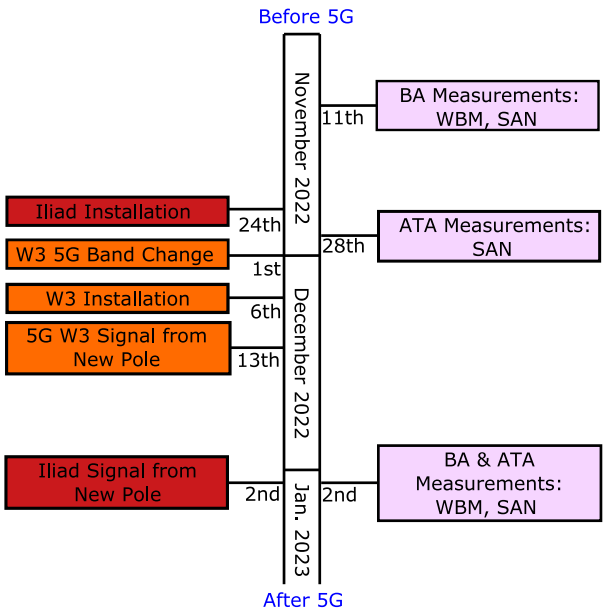

FIGURE 6. Timeline of measurement campaign and tower upgrade steps.

placed in close proximity to the directive antenna, obviously not obstructing the measurement antenna. In particular, such equipment is placed on a stone table in location 1 (Fig. 4(a)), while a camping table is employed for the other locations (Fig. 4(b)-4(d)). In this way, the connection between the SAN and the received antenna is simplified, yielding for example to a very low torque of the radio-frequency (RF) cable that avoids cable and connectors damages.

Focusing on the settings already implemented by default on the SAN, we set an RMS trace detector for NRT evaluations. When considering RT, we instead use a peak detector. This choice is motivated by the fact that the RMS trace detector is not available in RT mode. The detector type is set to rolling average for NRT, while a simple clear write is implemented in RT. The antenna factor vs. frequency table is pre-loaded on the SAN. In this way, the measured channel power can be directly expressed in terms of power density. The reference level and scale divisions are set to the default values of 65 [dBm/m^2] and 15, respectively, due to the fact that the signal dynamic range is unknown a-priori. Eventually, RBW and VBW are automatically tuned by the SAN, as reported in Table 2. Similarly, the number of frequency samples that are sensed during a single sweep is kept to the default values, namely 4001 for NRT and 501 RT, respectively, again in accordance with Table 2.

Focusing on NBMEA algorithm setting, the $\mathbb{F}$ input vector is set with the frequency column of Table 5 (W3 case) and Table 6 (Iliad case), respectively. The span input vector $\mathbb{S}$ is initialized with the band column of Table 5 (W3 case) and Table 6 (Iliad case), respectively. The initial waiting time T^{INIT} before producing the first channel power measurement is set to 2 [s], in order to allow a stabilization of the signal level. The time between one channel power measurement and the following one, denoted with T^{SAM}, is set to 0.5 [s].

FIGURE 7. Positioning of traffic chain (smartphone and tripod) and SAN chain (SAN, directive antenna, tripod, control laptop and cables) during ATA assessment.

Moreover, the number of channel power samples to compute the average is set to N^{SAM}=100. This value has also a beneficial effect on the stabilization of the recorded signal.

2) WBM CHAIN SETTINGS

The WBM meter is placed on a tripod, at a height of 1 [m] to avoid the detection of ground reflections, in line with similar settings already applied for the SAN directive antenna. The meter is then configured with the following settings: *i*) total measurement time equal to 6 [minutes], *ii*) type of average corresponding to a sliding window, *iii*) temporal extension of the sliding window set to 10 [s], *iv*) sampling rate set to 0.5 [s].

3) TRAFFIC CHAIN SETTINGS

Focusing on the traffic chain, we place the smartphone (either the Samsung S20+ 5G or the Apple iPhone 12) over a tripod, behind the main direction of the SAN antenna, at a horizontal distance of 1 m, as shown in Fig. 7. In this way, the SAN antenna correctly measures the DL EMF component, while the uplink (UL) radiation does not interfere with the measured data. The smartphone distance from the ground is set to 0.93 [m], in order to minimize the effect of ground reflections.

We then move our attention to the setting of the iPerf transfer. In this work, we select Transmission Control Protocol (TCP) as transport layer protocol, in order to allow the tuning of the data transfer speed in accordance with the available capacity. In addition, TCP automatically limits congestion effects that could introduce consistent packet losses - and consequently throughput decrease. We then impose a single TCP connection for the data transfer, with a time granularity for producing the iPerf output set to 1 [second] between consecutive measurements. Eventually, the reverse mode is activated, in order to impose traffic generation in the DL direction. Finally, the maximum transfer time is set to 180 [second], a period of time that we empirically found

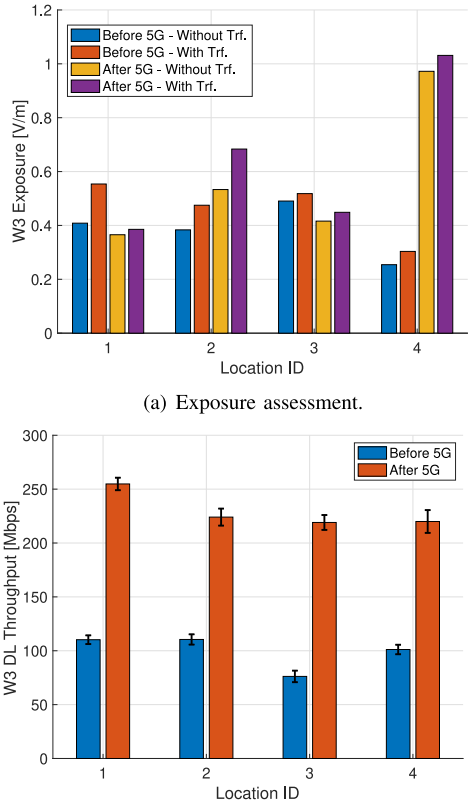

(a) Exposure assessment.

(b) Throughput assessment.

FIGURE 8. Exposure and throughput assessments of W3 operator (throughput error bars: confidence intervals computed with 95% confidence level computed from the output of iPerf App of the Samsung S20+ 5G smartphone).

to be sufficiently long to run the exposure data recording across the set of bands by the SAN chain.

C. W3 ANALYSIS

We initially focus on the main outcomes derived from the analysis of W3 operator. Fig. 8 reports the exposure assessment on top and the throughput assessment before and after 5G activation on bottom. Each bar in the subfigures correspond to the average exposure/throughput metric over the considered test. More specifically, each W3 exposure bar is obtained in the following way:

1) measurement of power density for each band of W3 operator by the SAN (W3 B or W3 A set of bands of Table 5, respectively);
2) computation of total W3 power density by summing up the measured power densities over the different set of bands (W3 B or W3 A);
3) transformation from power density to electric field (by assuming a free space wave impedance of 50 [Ohm])

In addition, the exposure assessment of Fig. 8(a) further differentiates among exposure without traffic (retrieved by running the BA procedure) and exposure with active traffic generated towards the measurement location (retrieved by running the ATA procedure).

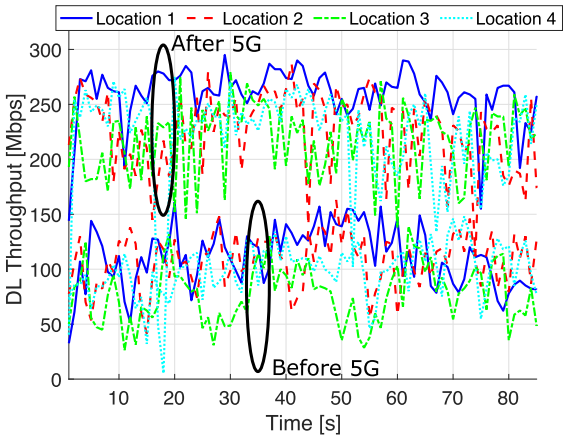

FIGURE 9. W3 DL Throughput vs. time over the different locations before and after 5G activation - figure best viewed in colors.

Focusing on the exposure assessment (Fig. 8(a)), the exposure does not considerably vary before and after 5G activation in almost all locations - except from location 4. For example, exposure tends to be slightly reduced when 5G is activated in location 1 and 3, while a modest increase of exposure is observed in location 2. Eventually, the relative strong increase in the exposure that is observed for location 4 is likely due to a change in the experienced propagation conditions, i.e., a semi-LoS obstructed by foliage from the pre-5G pole (Fig. 4(d)) to a complete LoS from the post-5G pole. However, another effect that may have an impact on the increase of exposure for location 4 is a variation in the received power from the main lobes towards the considered location.

When traffic is activated towards the measurement location, a local increase of exposure level is observed, both before and after 5G activation. This is an expected outcome, as 4G and 5G technologies are able to scale the radiated power of the transmitting antenna based on the traffic levels that are flown over the radio link. However, such increase of exposure is always rather thin, i.e., lower than 0.1 [V/m], for all the considered scenarios.

We then move our attention to the average throughput levels, shown Fig. 8(b). In this case, 5G activation triggers a prompt increase in the achieved throughput in all locations, passing from 80-10 [Mbps] to more than 200 [Mbps]. It is interesting to note that, despite the throughput is doubled in all locations, the exposure does not experience the same increase (except from location 4). Again, this is an important indication showing the efficiency of 5G in delivering large amount of data.

To give more insights, Fig. 9 reports the evolution of throughput levels vs. time over the different locations. As expected, minor throughput oscillations are observed, which may be due to the evolution of TCP congestion window. However, two distinct zones emerge, corresponding to the tests before 5G (lower throughput) vs. the ones after 5G (with higher throughput).

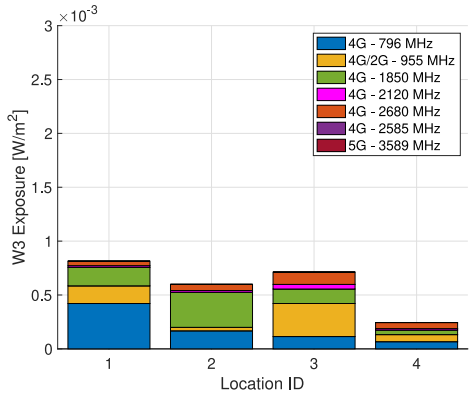

(a) Before 5G.

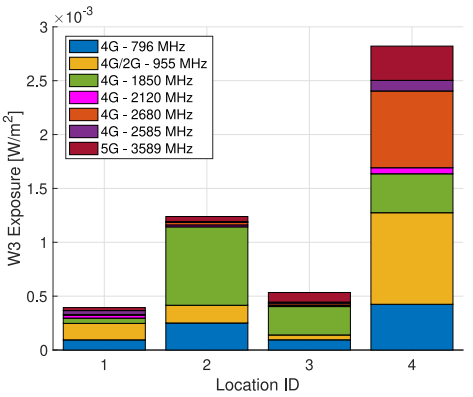

(b) After 5G.

FIGURE 10. Breakdown of exposure components before and after 5G provisioning - W3 operator (subfigures best viewed in colors).

In the following step, we provide more details about the exposure sources. To this aim, Fig. 10 reports the power density components over the different bands in pre-5G and after-5G conditions, obtained by running the ATA procedure. Before 5G activation, most of radiation is due to 4G, particularly for frequencies below 2 [GHz]. When 5G is activated, the signal on the 5G mid-band starts to be detected (as expected). However, the share of 5G component is overall rather tiny compared to the exposure of 4G bands, thus confirming that 5G always represents a small amount of exposure over the total one. Eventually, we point out that a subset of 4G bands (e.g., the one at 1850 [MHz]) may be used to dynamically share both 4G and 5G signals.

In the next part, we evaluate the efficiency before and after 5G activation in more detail. To this aim, we compute a novel metric, called exposure per Mbps, which is obtained by dividing average 5G exposure over average throughput for each location. Fig. 11 highlights the obtained outcomes. Interestingly, the exposure per Mbps is dramatically reduced upon 5G activation - except from location 4 that experiences a moderate increase. This outcome confirms the 5G efficiency in delivering more bits while at the same time limiting the exposure levels in almost all locations.

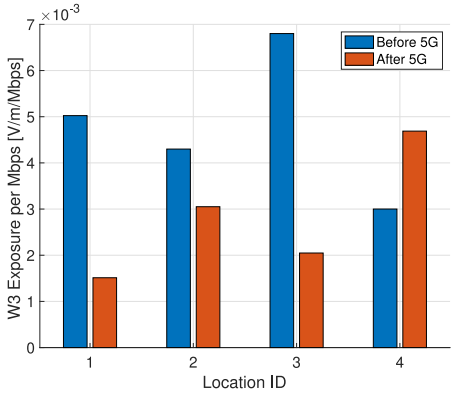

FIGURE 11. Exposure per Mbps metric of W3 operator.

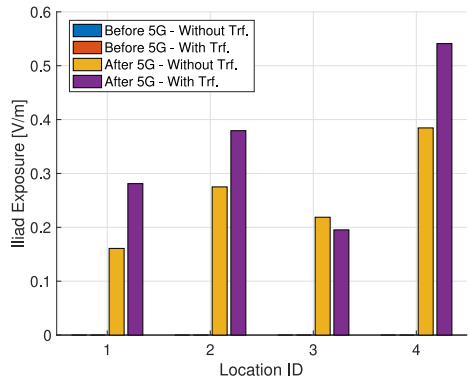

(a) Exposure assessment.

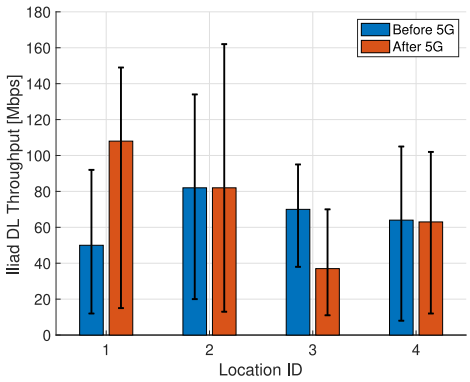

(b) Throughput assessment.

FIGURE 12. Exposure and throughput assessments of Iliad operator (throughput error bars: minimum and maximum throughput values provided by iPerf App on iPhone 12 smartphone).

D. ILIAD ANALYSIS

We now repeat the selective analysis by focusing on the Iliad operator. Fig. 12 reports the Iliad exposure and throughput variations. Several considerations hold by analyzing the figure. First, Iliad exposure before 5G activation was not detected by the SAN antenna, which was pointed towards the pre-5G pole. This is an expected outcome, as the exposure over the measurement locations was likely generated by other Iliad installation(s) deployed over the territory. Second,

5G activation does not dramatically impact the throughput levels - except from location 1, which experiences a steadily increase of speed. The relative throughput stability in the other locations may be explained by the bands that are adopted to provide mobile service (shown in Table 6). In particular, the band allocation before and after 5G activation is not substantially varied, except from the 5G band. Differently from W3, however, the 5G band activated by Iliad is lower in terms of frequency and narrower in terms of spectrum occupation. This fact, coupled by the exploitation of passive antennas to spread the 5G signal,[3] corroborates our intuition that Iliad mainly ensures coverage rather than capacity with the installed 5G antennas.

E. JOINT ANALYSIS

We then move our attention to the analysis of total exposure levels in the following cases:

1) total exposure of W3 and Iliad operators with ATA procedure (SAN chain);
2) total exposure of all the sources with BA procedure (WBM chain).

Focusing on *1*), Fig. 13(a) reports the achieved exposure levels over the different locations. Interestingly, the total exposure is not substantially affected by 5G in location 1 and 3. On the other hand, a local increase of exposure is observed for location 2 and location 4, respectively. Interestingly, such increase of exposure is mainly due to the exposure variations observed on W3 measurements (Fig. 8(a)).

Focusing on *2*), Fig. 13(b) highlights the outcome of WBM chain (BA assessment). Naturally, the exposure in Fig. 13(b) is higher than the one in Fig. 13(a), since the former is measured through a tri-axial probe - which integrates multiple exposure components from all the nearby sources (e.g., installations from other operators) - while the latter is retrieved by employing a directive antenna over the set of W3 and Iliad bands. However, it is interesting to note that location 1 and 3 generally experience a decrease of exposure before and after 5G activation in both assessments.

F. 5G SPECTRUM ANALYSIS

Up to this point, a natural question is: At what extent 5G is used on the considered 5G bands? To answer such question, we perform an analysis of the spectrum occupancy of the used 5G bands in post-5G scenarios, tailored to W3 and Iliad operators.

1) W3 SPECTRUM

Waterfall Diagrams: We initially record in RT the waterfall diagram with the SAN chain, by considering the 5G spectrum portion of W3 over mid-band frequencies. Fig. 14 reports the obtained results in the following cases: *i*) without traffic

3. A passive antenna does not implement multiple-input multiple-output (MIMO) and beamforming functionalities, which are instead provided by active 5G antennas.

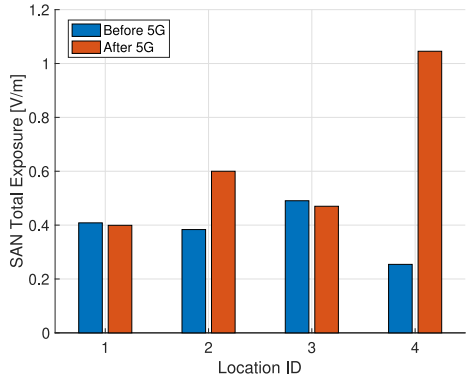

(a) SAN Measurement Chain

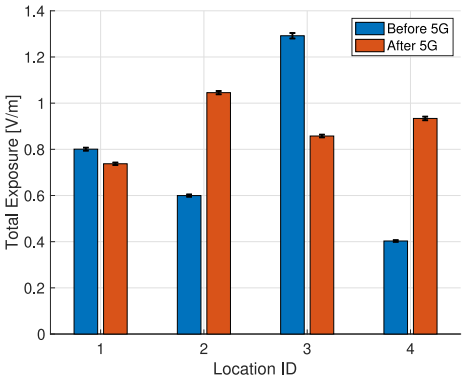

(b) WBM Measurement Chain.

FIGURE 13. Total exposure from the different chains (WBM measurement chain error bars: confidence intervals computed from EMF traces with a confidence level of 95%).

(Fig. 14(a)), and *ii*) with injected traffic (Fig. 14(b)). The x-axis is the frequency domain, while the y-axis is the time domain (with measurement time set to 60 [s] in both cases). The color of each pixel in the subfigure is proportional to the strength in the received power level: brighter for higher power, darker for lower power, degrading to blue and black colors for values close to the noise level. In both cases, a vertical strip of relatively unused spectrum portion appears on the left. This zone is intentionally unused by the operator, in order to align effective employed bandwidth with the size defined by 3rd Generation Partnership Project (3GPP) standards - set to 60 MHz in this case. In a similar way, another blue strip (narrower than the one on the left) appears on the right, indicating that the frequencies close to the upper border of the W3 spectrum are not used to avoid interference with the adjacent band that is licensed to another operator.

In the following, we focus on the central part of the figures, in which the signal power is always non-negligible. Interestingly, the traffic activation triggers a prompt increase in the received power (Fig. 14(b)). On the other hand, when traffic is not injected towards the measurement location, the received power is substantially lower (Fig. 14(a)). This effect is due to the following reasons: *i*) no other nearby terminals are used during this step, and hence no traffic

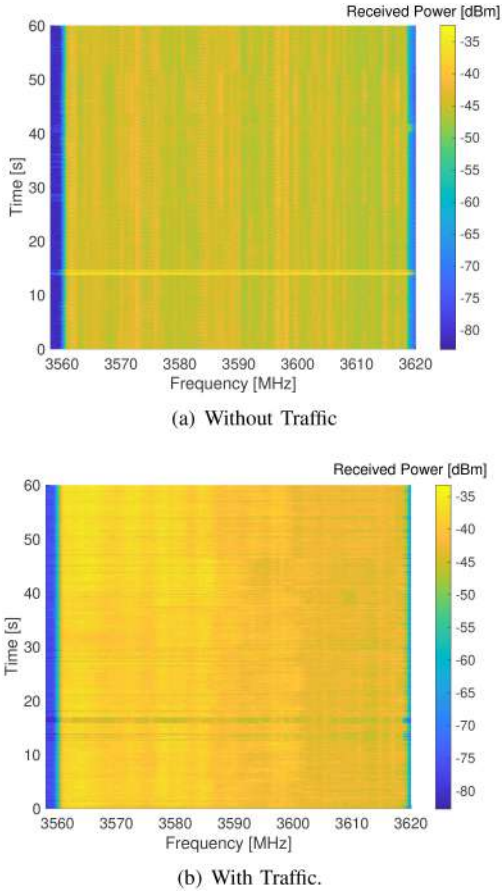

FIGURE 14. RT waterfall diagrams of 5G W3 spectrum without and with injected traffic (subfigures best viewed in colors).

beams are oriented towards the measurement location, *ii*) the amount of 5G traffic generated by other users is substantially very low.

Eventually, the spectrum usage in the central part of Fig. 14(b) is not uniform. In particular, the brighter color on the left of the plot reveals that the operator preferentially assigns radio resource elements from left to right of the spectrum, thus prioritizing lower frequencies in the radio resource management step. This choice may be motivated by the fact that the propagation loss increases with the adopted frequency, and hence lower frequencies introduce a smaller loss.[4]

Persistence Analysis: In the following step, we analyze the persistence of the 5G signal. This metric is a peculiar feature that is made available on the SAN screen in RT mode. Fig. 15(a) and Fig. 15(b) report the SAN screenshots without and with injected traffic, respectively. The yellow line in each plot is the snapshot of the instantaneous spectrum (with clear/write trace detector), while the color within the spectrum represents the signal persistence over time. When the signal maintains a given power value over time, the

4. We remind in fact that one term of commonly used propagation loss models is $20 \cdot \log 10(f)$, where f is the adopted frequency.

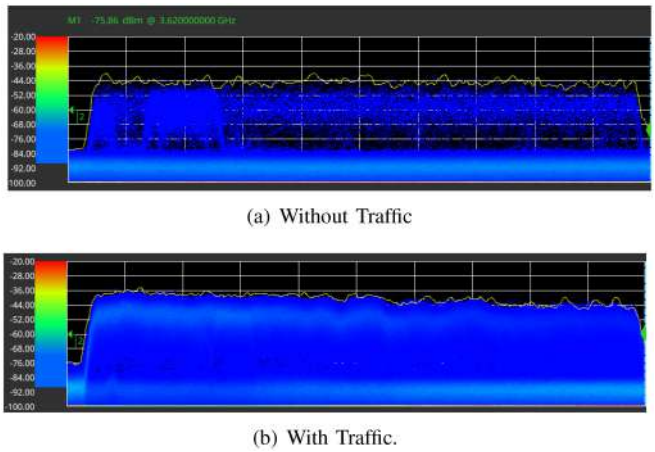

FIGURE 15. RT SAN output of 5G W3 spectrum without and with injected traffic (subfigure best viewed in colors).

persistence color turns to blue and eventually light blue for very stable signals.

When considering the case without traffic (Fig. 15(a)), the color persistence reveals three distinct behaviors, namely: *i*) a flat signal persistence to values close to noise level (indicating that most of the time the 5G signal is very low), *ii*) a stronger portion on top left part of the signal, revealing the presence of control channels (mainly Synchronization Signal Block (SSB)) - which are regularly transmitted at constant power, *iii*) a light persistence on top part of the spectrum (left to right), indicating that the band is also sometimes used to carry background traffic to other users.

The generation of traffic notably varies the spectrum persistence, as shown in Fig. 15(b). In more detail, the blue color spread within the spectrum reveals that the signal intensity is increased compared to the case without traffic. In addition, the bright color on top left indicates that the spectrum is preferentially used to transport traffic data on the measurement location. However, the signal also oscillates among high and low values. This behavior is a consequence of TDD functionality, in which DL and UL slots are multiplexed in the time domain. Obviously, in our case, the DL slots are filled with traffic, while the UL ones are not substantially used (except from carrying light TCP acknowledgements). Consequently, the spectrum persistence is not negligible also for lower values - even close to noise level - corresponding to TDD slots with no or very low UL traffic.

Statistical Analysis: We then move our attention to the characterization of the spectrum statistics taken in real time. More concretely, Fig. 16(a) shows the average spectrum over the one-minute window collected without and with injected traffic respectively. Interestingly, the traffic generation tends to affect the left part of the spectrum, which is even higher than 5 [dB] compared to the case without traffic. On the other hand, the spectrum increase due to traffic is less evident on the right part of the spectrum, thus suggesting that the radio resources are preferentially assigned starting from lower spectrum frequencies towards higher ones. The figure

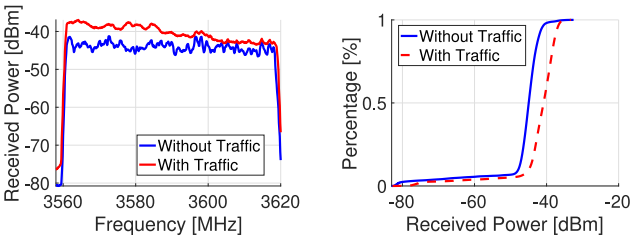

(a) Average Spectrum. (b) ECDF of the received power.

FIGURE 16. Analysis of 5G W3 spectrum and received power without and with injected traffic.

is then complemented by Fig. 16(b), which shows the empirical cumulative distribution function (ECDF) of the received power samples. Interestingly, the traffic generation shifts the ECDF to the right. Moreover, a small percentage of samples (appearing on bottom part of the plot) are not substantially affected by traffic. These data correspond to the samples falling within the guard bands on the spectrum sides, which are unused and consequently experience negligible received power values.

2) ILIAD SPECTRUM

Waterfall Diagrams: Fig. 17 reports the RT waterfall diagram of 5G Iliad spectrum at 700 [MHz]. Differently from W3, the traffic generation towards the measurement location does not substantially affect the waterfall trend. In more detail, the waterfall colors are very similar in Fig. 17(a)-Fig. 17(b)), thus indicating that the traffic generation does not have a substantial effect on the measured spectrum. This behavior reveals a different usage of such spectrum portion by Iliad. In particular, the relatively strong utilization of the spectrum in the case without traffic (shown in Fig. 17(a)) suggests that such 5G band is in reality used to transport 4G signals, which are used by other terminals spread within the coverage area of the cell.

Statistical Analysis: In the final part of our work, we compute the average Iliad spectrum without and with generated traffic, as shown in Fig. 18(a). The figure confirms the waterfall findings, namely a spectrum invariance over the two tests. Eventually, the ECDF shown in Fig. 18(b) reveals a very small increase in the received power (lower than 1 [dB]) upon traffic activation.

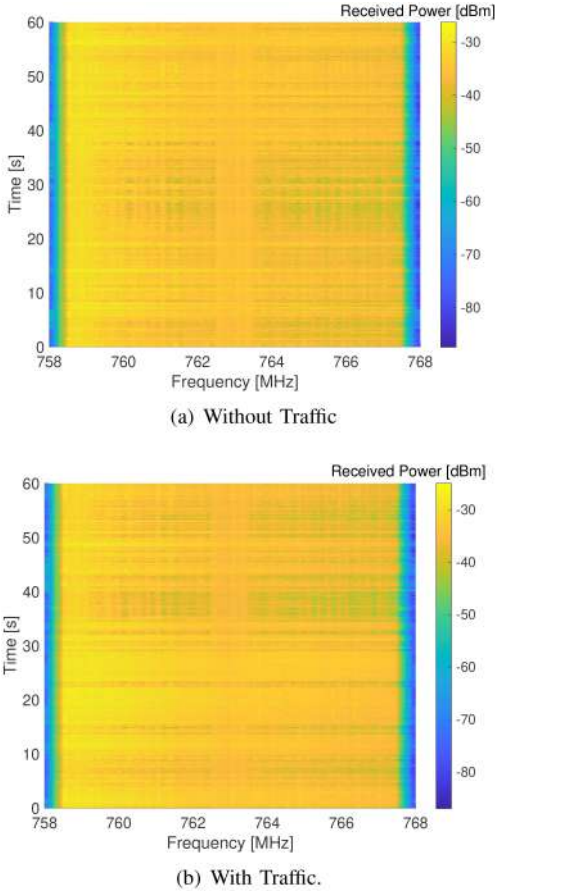

(a) Without Traffic

(b) With Traffic.

FIGURE 17. RT waterfall diagrams of 5G Iliad spectrum without and with injected traffic (subfigures best viewed in colors).

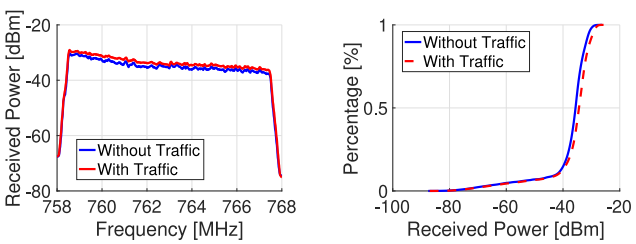

(a) Average Spectrum. (b) ECDF of the received power.

FIGURE 18. Analysis of 5G Iliad spectrum and received power without and with injected traffic.

VI. CONCLUSION AND FUTURE WORK

We have targeted the problem of assessing the impact of 5G by performing EMF and throughput measurements before and after 5G activation. To meet such goal, we have designed an innovative measurement framework, based on the exploitation of SAN and WBM exposure assessment chains and one traffic generation chain. In addition, we have implemented the innovative NBMEA algorithm to remotely control the measurement steps on the SAN chain. We have then performed a set of detailed measurements with our framework over the territory, before and after the activation of 5G signals by two operators. Results demonstrate that the activation of 5G over mid-bands is effective in improving the throughput levels, which easily reach values above 200 [Mbps]. In addition, the exposure levels are not substantially varied compared to the pre-5G case, apart from a specific location that experiences an improvement in the sight conditions. Moreover, the activation of 5G over the sub-GHz band does not affect the throughput, mainly because such spectrum is in reality employed to provide coverage and to carry background 4G traffic.

As future work, we plan to extend the considered evaluation to other deployments, including mm-Wave frequencies.

Such bands need to be monitored (despite their relatively low usage), due to the potential large throughput levels that can be provided. In addition, the application of our framework to other nations is a very interesting area of research. Such countries may enforce different power radiation patterns (due, e.g., to less stringent exposure regulations) that could yield to potentially higher exposure levels than the ones observed in this work. Moreover, the exposure assessment from multiple terminals used in parallel is another avenue of research, mainly because the composite exposure levels may increase compared to our outcomes. Finally, we plan to focus on a portion of territory in which 5G is activated through a set of small cells, in order to study the impact of a dense deployment on exposure and traffic levels.

ACKNOWLEDGMENT

The authors would like to thank Dr. Jack Rowley for the fruitful suggestions during paper preparation.

REFERENCES

[1] "Forum MobilKommunikation—Cellular measurement series. Security. Transparency. Responsability." Accessed: Feb. 21, 2023. [Online]. Available: https://fmk.at/wp-content/uploads/2022/05/FMK_Messbroschure_2022-1.pdf

[2] M. Nedelcu, T. Petrescu, and V. Nițu, "Evaluation of electromagnetic field exposure in the vicinity of mobile phone base stations," in *Proc. IEEE Int. Black Sea Conf. Commun. Netw. (BlackSeaCom)*, 2021, pp. 1–5.

[3] A. C. Markussen, T.-M. Sjoemoen, E. H. Unander, and L. Klaeboe, "Regular measurements of EMF in a representative Norwegian city-constant exposure over time despite introduction of new technologies," *Environ. Monitor. Assess.*, vol. 194, no. 10, p. 694, 2022.

[4] "Study of the 5G contribution to exposure of the general public to electromagnetic waves." Accessed: Feb. 21, 2023. [Online]. Available: https://www.anfr.fr/fileadmin/mediatheque/documents/expace/20211214-exposition-5G-EN.pdf

[5] "Assessment of the exposure of the general public to 5G electromagnetic waves—Part 1." Accessed: Feb. 21, 2023. [Online]. Available: https://www.mca.org.mt/sites/default/files/MCA_R_21_4441_Assessment%20of%20the%20exposure%20of%20the%20general%20public%20to%205G%20electromagnetic%20waves%20_Part%201_0.pdf

[6] L.-M. Schilling, C. Bornkessel, and M. A. Hein, "Analysis of instantaneous and maximal RF exposure in 4G/5G networks with dynamic spectrum sharing," in *Proc. 16th Eur. Conf. Antennas Propag. (EuCAP)*, 2022, pp. 1–5.

[7] S. Aerts et al., "In-situ measurement methodology for the assessment of 5G NR massive MIMO base station exposure at sub-6 GHz frequencies," *IEEE Access*, vol. 7, pp. 184658–184667, 2019.

[8] S. Adda et al., "A theoretical and experimental investigation on the measurement of the electromagnetic field level radiated by 5G base stations," *IEEE Access*, vol. 8, pp. 101448–101463, 2020.

[9] S. Aerts et al., "In situ assessment of 5G NR massive MIMO base station exposure in a commercial network in Bern, Switzerland," *Appl. Sci.*, vol. 11, no. 8, p. 3592, 2021.

[10] L. Chiaraviglio et al., "Massive measurements of 5G exposure in a town: Methodology and results," *IEEE Open J. Commun. Soc.*, vol. 2, pp. 2029–2048, 2021.

[11] B. Selmaoui, P. Mazet, P.-B. Petit, K. Kim, D. Choi, and R. de Seze, "Exposure of South Korean population to 5G mobile phone networks (3.4–3.8 GHz)," *Bioelectromagnetics*, vol. 42, no. 5, pp. 407–414, 2021.

[12] S. Q. Wali, A. Sali, J. K. Allami, and A. F. Osman, "RF-EMF exposure measurement for 5G over mm-wave base station with MIMO antenna," *IEEE Access*, vol. 10, pp. 9048–9058, 2022.

[13] L. Chiaraviglio et al., "EMF exposure in 5G standalone mm-Wave deployments: What is the impact of downlink traffic?" *IEEE Open J. Commun. Soc.*, vol. 3, pp. 1445–1465, 2022.

[14] D. Colombi, F. Ghasemifard, P. Joshi, B. Xu, C. Di Paola, and C. Törnevik, "Methods and practices for in situ measurements of RF EMF exposure from 5G millimeter wave base stations," *IEEE Trans. Electromagn. Compat.*, vol. 64, no. 6, pp. 1986–1993, Dec. 2022.

[15] M. S. Elbasheir, R. A. Saeed, and S. Edam, "Measurement and simulation-based exposure assessment at a far-field for a multi-technology cellular site up to 5G NR," *IEEE Access*, vol. 10 pp. 56888–56900, 2022.

[16] M. Ursăchianu, C. Lăzărescu, O. Bejenaru, and A. Sălceanu, "Assessment of human exposure to EMF generated by 5G mobile phone base stations," in *Proc. IOP Conf. Ser. Mater. Sci. Eng.*, 2022, Art. no. 12026.

[17] N. Djuric, N. Kavecan, N. Radosavljevic, and S. Djuric, "The wideband approach of 5G EMF monitoring," in *Proc. 12th EAI Int. Conf. AFRICOMM*, Mar. 2021, pp. 86–98.

[18] N. Djuric, D. Kljajic, T. Gavrilov, V. Otasevic, and S. Djuric, "The EMF exposure monitoring in cellular networks by Serbian EMF RATEL system," in *Proc. IEEE Int. Symp. Measur. Netw. (M N)*, 2022, pp. 1–6.

[19] L. Chiaraviglio, C. Lodovisi, D. Franci, S. Pavoncello, and T. Aureli, "Six months in the life of a cellular tower: Is 5G exposure higher than pre-5G one?" in *Proc. IEEE Int. Symp. Meas. Netw. (M N)*, 2022, pp. 1–6.

[20] X. Yuan, S. Hu, W. Ni, R. P. Liu, and X. Wang, "Joint user, channel, modulation-coding selection, and RIS configuration for jamming resistance in multiuser OFDMA systems," *IEEE Trans. Commun.*, vol. 71, no. 3, pp. 1631–1645, Mar. 2023.

[21] S. Hu, X. Yuan, W. Ni, and X. Wang, "Trajectory planning of cellular-connected UAV for communication-assisted radar sensing," *IEEE Trans. Commun.*, vol. 70, no. 9, pp. 6385–6396, Sep. 2022.

[22] *Determination of RF Field Strength, Power Density and SAR in the Vicinity of Radiocommunication Base Stations for the Purpose of Evaluating Human Exposure*, Standard IEC 62232:2017. Accessed: Mar. 8, 2022. [Online]. Available: https://webstore.iec.ch/publication/28673

[23] "Case studies supporting IEC 62232—Determination of RF field strength, power density and SAR in the vicinity of radiocommunication base stations for the purpose of evaluating human exposure," IEC, Geneva, Switzerland, Rep. IEC TR 62669:2019. Accessed: Mar. 8, 2022. [Online]. Available: https://webstore.iec.ch/publication/62014

[24] "ATDI HTZ communications." Accessed: Mar. 14, 2023. [Online]. Available: https://atdi.com/products-and-solutions/htz-communications/

LUCA CHIARAVIGLIO (Senior Member, IEEE) received the Ph.D. degree in telecommunication and electronics engineering from the Politecnico di Torino, Italy. He is currently an Associate Professor with the University of Rome "Tor Vergata," Italy. He has coauthored more than 160 articles published in international journals, books, and conferences. His current research topics cover 5G and B5G networks, optimization applied to telecommunication networks, electromagnetic fields, and health risks assessment of 5G and B5G communications. He received the Best Paper Award at the IEEE Vehicular Technology Conference (VTC)-Spring 2020, the IEEE VTC-Spring 2016, and the Conference on Innovation in Clouds, Internet and Networks 2018, all of them appearing as the first author. Some of his papers are listed as the Best Readings on Green Communications by the IEEE. Moreover, he has been recognized as an Author in the Top 1% Most Highly Cited Papers in the Information and Communication Technology field worldwide and top 2% world scientists according to the 2021 and 2022 updates of the science-wide author databases of standardized citation indicators.

STEFANIA BARTOLETTI received the Laurea degree (summa cum laude) in electronics and telecommunications engineering and the Ph.D. degree in information engineering from the University of Ferrara, Ferrara, Italy, in 2011 and 2015, respectively. She is currently an Assistant Professor with the University of Rome "Tor Vergata," Italy. She was a Marie Skłodowska-Curie Global Fellow within the Horizon 2020 European Framework for a research project with the Wireless Information and Network Sciences Laboratory, Massachusetts Institute of Technology, Cambridge, MA, USA, and the University of Ferrara from 2016 to 2019. Her research interests include theory and experimentation of wireless networks for passive localization and physical behavior analysis. She was the recipient of the 2016 Paul Baran Young Scholar Award of the Marconi Society. She served as the Chair of the TPC for the IEEE ICC and Globecom Workshops on Advances in Network Localization and Navigation from 2017 to 2021 and a reviewer for numerous IEEE journals and international conferences. She is an Editor of the IEEE COMMUNICATIONS LETTERS.

NICOLA BLEFARI-MELAZZI is a Full Professor of Telecommunications with the University of Roma Tor Vergata, where he served as the Chair of the Ph.D. program in Telecommunications Engineering, the undergraduate and graduate programs in Telecommunications Engineering, and the Department of Electronic Engineering. From January 2017 to January 2023, he was the Director of CNIT (National Inter-University Consortium for Telecommunications), a nonprofit Consortium made up of 41 Italian Universities. Since January 2023, he has been the President of CNIT. His research projects have been funded by Italian Ministries, the Italian National Research Council, major companies (e.g., Ericsson and Telecom Italia), the ESA, and the EU. He has participated in 33 EU projects, playing the role of Project Coordinator and PI for seven of them. He is/has been a member of the board of the 5G Infrastructure Association and 6G Infrastructure Association. He has been appointed by the Ministry of University and Research as Italian representative in the Member States' Representatives Group of EU Programme on Smart Networks and Services Joint Undertaking. Since September 2022, he has been the President of the RESTART Foundation, established primarily for the implementation, coordination, and management of the 116 MEUR MUR-funded research program "Telecommunications of the Future." He is the author/coauthor of about 260 papers. His research interests lie in the performance evaluation, design, and control of telecommunications networks. He evaluated many research proposals and projects in EU programs and served as a TPC member, TPC chair, general chair, and steering committee chair for IEEE conferences and a guest editor for IEEE journals. He is an Area Editor of *Computer Networks* (Elsevier).

CHIARA LODOVISI received the Ph.D. degree in engineering electronics from the University of Rome Tor Vergata, Italy. She worked for five years as an RF Engineer Consultant for H3G mobile operator and then as a Research Associate with the University of Rome Tor Vergata, focusing on optical communications, submarine and satellite optical links, and radio over fiber. She is currently a Researcher with CNIT, Italy. Her research interests include 5G networks, health risk assessment of 5G communications, interoperability over fiber between TETRA/LTE systems, and 5G networks.

ALESSIA MORETTI graduated in modern literature from the University of Rome Sapienza. She is a Screenwriter and an Editor. She has collaborated on a cinematographic and television level with various production companies.

FRANCESCO ZAMPOGNARO received the M.Sc. degree in telecommunication engineering from the University of Rome "La Sapienza," Rome, Italy, in 2004, and the Ph.D. degree in space systems and technologies from the University of Rome "Tor Vergata," Rome, in 2010. He is currently a Researcher with the University of Rome "Tor Vergata," and a Professor of Space Systems with University Marconi, Rome. He teaches with Linux Management and Configuration Laboratory, MATLAB for Signal theory and Satellite Systems classes. He is the Co-Founder of RomARS srl, Rome, an innovative startup dealing with advanced telecommunication technologies. His research interests include satellite systems, supporting many research funded projects, and study and simulation of satellite systems, in particular DVB-RCS, covering protocols optimization, services provision and QoS, virtualization, security, resource allocation, integrated/hybrid architectures, and 5G.

MOHAMED-SLIM ALOUINI (Fellow, IEEE) was born in Tunis, Tunisia. He received the Ph.D. degree in electrical engineering from the California Institute of Technology, Pasadena, CA, USA, in 1998. He served as a Faculty Member with the University of Minnesota, Minneapolis, MN, USA, then with Texas A&M University at Qatar, Doha, Qatar, before joining the King Abdullah University of Science and Technology, Thuwal, Makkah Province, Saudi Arabia, as a Professor of Electrical Engineering in 2009. His current research interests include modeling, design, and performance analysis of wireless communication systems.

Open Access funding provided by 'Università degli Studi di Roma "Tor Vergata"' within the CRUI CARE Agreement